Interferometry with a dense 3D dataset

Fan-Chi Lin, Dunzhu Li, and Robert W. Clayton[*], Seismological Laboratory, California Institute of Technology, and Dan Hollis, NodalSeismic LLC.

Summary

In this paper we report on progress using ambient noise correlation with a dense 3D survey conducted in Long Beach, California, to estimate subsurface velocity. We show that both Rayleigh wave and body wave signals can be clearly observed between 0.2-10 Hz frequency range in the noise cross-correlations. The observed signals also compare well with an active source gather. We apply eikonal tomography to invert for the Rayleigh wave phase velocity maps at several different frequencies. The phase velocity maps, which are most sensitive to structure in the top 600 meters, show clear correlation with known surface features such as the slow anomaly adjacent to the coast in the south and a fast anomaly associated with the Newport-Inglewood fault zone. The results presented in this study show the potential of using ambient noise interferometry method to complement active source techniques in studying high-resolution shallow crustal structure.
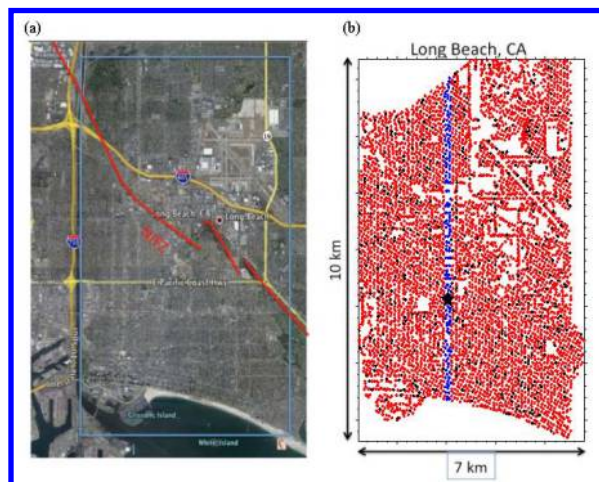

Figure 1. (a) The deployment area of the 3D array used in this study is outlined in the Long Beach area. The Newport-Inglewood fault zone (NIFZ) is denoted by the red lines. (b) The station locations are shown as red dots. The black dots show the location of 500 virtual sources where cross-correlation to all other stations have been calculated. The star shows the example virtual source used in Figures 3 and 4. The blue dots mark the location of stations used in Figure 3c-d.

Introduction

Seismic interferometry or ambient noise cross-correlation method has now become an important tool to image shallow earth structure (e.g. Sabra et al. 2005; Shapiro et al. 2005; Lin et al. 2011). The method extracts seismic waves propagating between two arbitrary seismic stations by cross-correlating continuous noise recorded at the two stations. While the method is commonly used in studying crust and upper mantle structure based on surface wave observations (e.g. Lin et al. 2008; Moschetti et al. 2010), there is a growing interest body waves (e.g. Zhan et al. 2010; Poli et al. 2011) and exploration geophysics applications (e.g. Draganov et al. 2006; Draganov et al. 2009; Ruigrok et al. 2011).

In this presentation, we demonstrate that the ambient noise cross-correlation technique can be successfully applied to an exploration seismic array to extract both surface wave and body wave signals. The dataset consists of continuous recordings from approximately 5200 vertical velocity seismometers with a nominal pass band of 3-250 Hz, deployed in a 7x10 km region of city of Long Beach, CA, during the first six months of 2011. We show that by using ten days of continuous noise records, the cross-correlations between a station and all other stations can be used to construct seismic wave field emitted by a virtual source located at that station. The body wave signals are relatively weak in each individual cross-correlations, but the Rayleigh wave signals are strong enough for travel time measurement and tomography applications. We apply Eikonal tomography to construct 2D Rayleigh-wave phase-velocity maps and demonstrate the potential of applying ambient noise tomography to determine the 3D velocity structure.

Theory and Method

With seismic interferometry, we attempt to estimate the Green's functions by the well-known correlation equation

$$G_{ij}(t) - G_{ji}(-t) = -\frac{\partial}{\partial t} u_i \otimes u_j / S_i S_j \quad (1)$$

where u_i and u_j are the seismograms recorded at the ith and j^{th} sensors respectively and G_{ij} is the Green's function between the two locations and G_{ji} it is reciprocal (Lobkis and Weaver, 2001; Sneider, 2004). To accurately determine the Green's functions, it is necessary to deconvolve the ambient-noise source-spectra (S_i and S_j) for each station. In its simplest form, this is a temporal deconvolution and is often implemented as a whitening operator (Prieto et al. 2011; Benson et al. 2007). More generally, the anisotropic behavior as well as non-equal partitioning of the energy with ray parameter should also be compensated. In the results we present here, we average the signals observed in
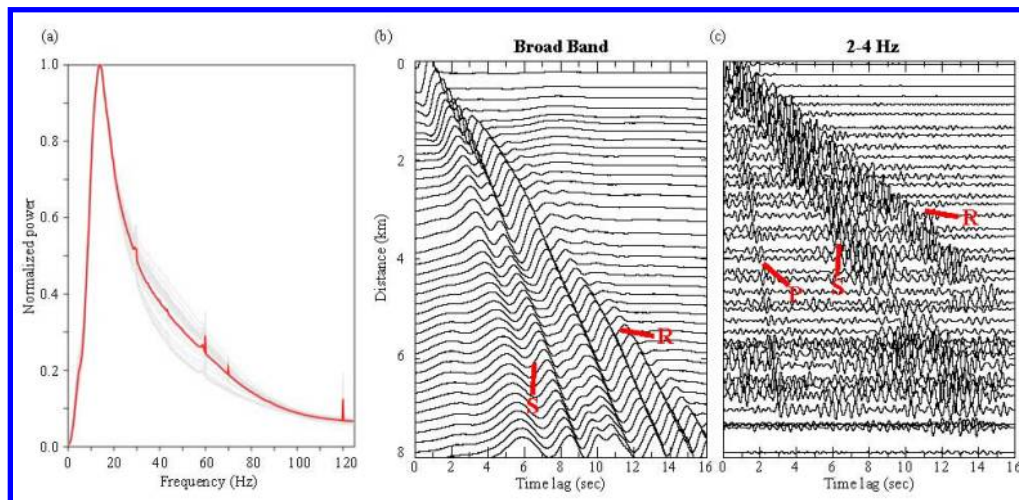
Figure 2. (a) Average spectrum of all receivers averaged over one day. The light gray lines show hourly variations. (b) Broad-band stacked cross-correlation record section. (c) 2-4 Hz bandpass-filtered cross-correlation record section.

positive and negative lags of cross-correlation and implement spectral whitening. Since the cross-correlations are calculated and normalized for each 15-minute interval before stacking, large impulsive events such earthquakes are naturally suppressed (Prieto et al., 2011).

In Figure 2a, we show the raw signal spectrum determined for a 24-hour period averaged over all 5200 stations. The sharp roll-off at 0-3 Hz is due to filters applied in the recorders, although we found that we had useful signal down to 0.1Hz, which is lower limit of interest because at this frequency, the wavelength is approximately the size of the survey itself. Note that there is no evidence of the active vibrator source (8-80 Hz sweep), which was active for several of the hours when the spectra were estimated.

Due to the significant amount of data, we only present the preliminary result based on cross-correlation between 500 central stations (Figure 1b) to all other ~5200 stations for all noise recorded during the first 10 days of May, 2011. In Figure 2b, these cross-correlations are stacked in 200 m path-distance bins and are shown as a record section. Clear Rayleigh wave and S wave signals with dominant frequency near 0.5-1 Hz are observed. Compare to Fig. 2a, the stronger low-frequency signals observed in the cross-correlations are likely due to higher attenuation and smaller stationary phase area (Sneider, 2004) at higher frequency. In the frequency band and distances that we consider here, the S-wave and higher-mode surface waves behave similarly and are difficult to distinguish with single component records.

While only Rayleigh and S waves are observed in Figure 2b, a clear P wave signals can also be observed in the 2-4 Hz frequency band. At this frequency band, the P wave which propagates at ~2km/s is better separated from the dominant Rayleigh wave and S wave signals. The ability to observe P, S, and Rayleigh waves is important for using ambient noise cross-correlation to invert for 3D structure beneath the array.

Virtual Source

To extend the correlations such as those shown in Fig. 2b-c to the problem of determining the 3D structure requires the wavefield to be estimated at every location. Based on the relationship between cross-correlation and the Green's function as suggested in equation (1), the cross-correlations between one center station and all other stations can be used to represent wave field emitted by a virtual source located at the center station location. In Figure 3a-b, two time snapshots of the wavefield emitted by a virtual source near the center of the network are shown. Clear Rayleigh and S-wave signals can be observed along with a weak P-wave. The figure also shows the anisotropic nature of the raw Green's function estimates. Noise sources are particularly strong on the oceanic sides, namely south and west, where strong Rayleigh wave noise signals are emitted by interaction between ocean wave and the sea floor (Stehly et al. 2006).
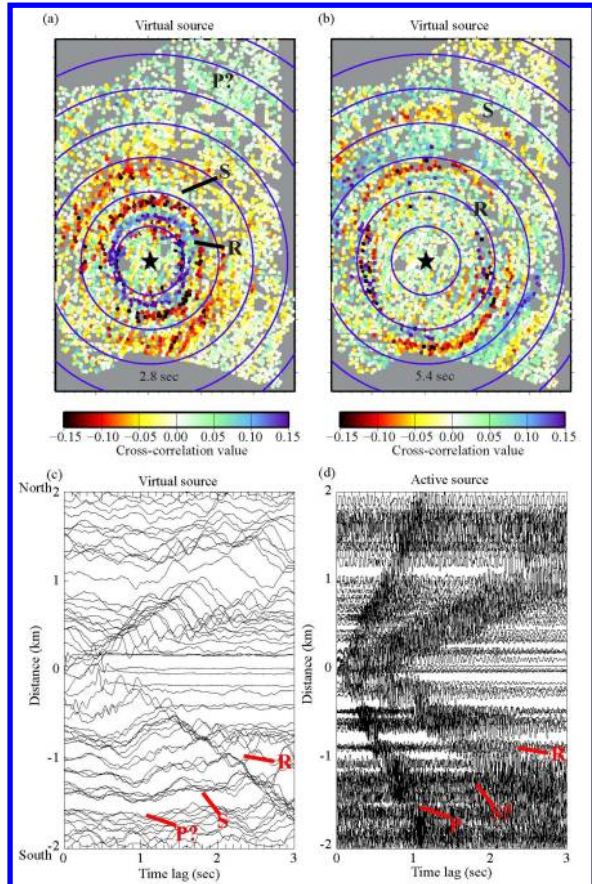
Figure 3. (a)-(b)Time slices of a virtual source. Contour interval is 1 km. (c)-(d) Comparison of virtual source and vibrator source.

In Figure 3c-d, a comparison between a virtual source gather and a vibrator-source gather at the same point are shown (corresponding to the north-south line of stations shown as blue dots in Figure 1). The vibrator gather shows a P and Rayleigh arrival. The move out of the P wave, ~2 km/s, agrees well with the result shown in Fig. 2c, based on stacked ambient noise cross-correlations. The virtual source has a Rayleigh wave and a weak P-wave although the signals have lower frequency than with the vibrator source. The S-wave is not separated from the Rayleigh wave in the distance range we plotted here. The decay of signal strength with offset is comparable between the two sources.

Eikonal tomography

With the correlations presented here, the body wave signals are too weak to perform a 3D tomographic inversion. However, we demonstrate the potential of using the Rayleigh-wave signals observed in the cross-correlations to estimate the shallow S-wave velocity. The technique we applied is called Eikonal tomography which measures the horizontal phase speeds of surface waves based on the Eikonal equation (Lin et al., 2009; Lin et al., 2011; Ritzwoller et al., 2011)

$$|\nabla\tau(x_i, x)|^2 = 1/c^2(x) \qquad (2)$$

where τ is the travel time between the virtual source point x_i and receiver at x.

We apply frequency-time analysis (FTAN) (Lin et al. 2007; Lin et al., 2008) to measure Rayleigh wave phase travel times between each virtual source and all other stations. A minimum curvature surface fitting (Smith & Wessel, 1990) is then applied to interpolate travel time measurements onto a regular grid (200 ft node spacing), before the spatial gradient in equation (2) is calculated. An example of 0.66 Hz Rayleigh wave phase travel time surface for the virtual source using in Figure 3 is shown in Figure 4. Travel time increases with distance as expected although the map is less reliable in regions with weaker surface wave signals (e.g. east; see Figure 3a-b).
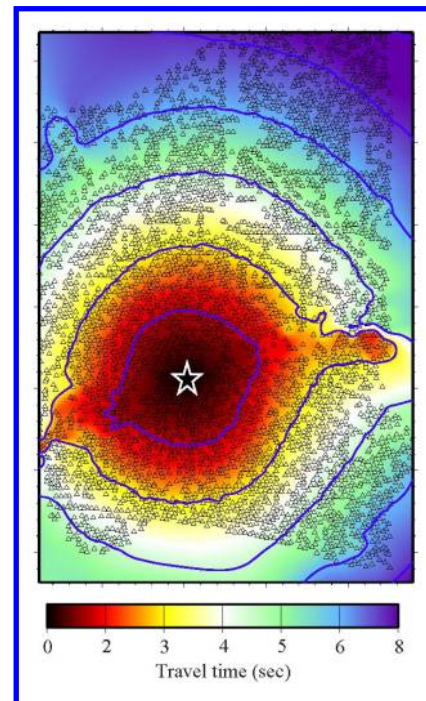

Figure 4. Rayleigh wave phase travel time surface. The contours are 1.5-sec travel time intervals. The phase velocity can be estimated by the gradient of this surface.
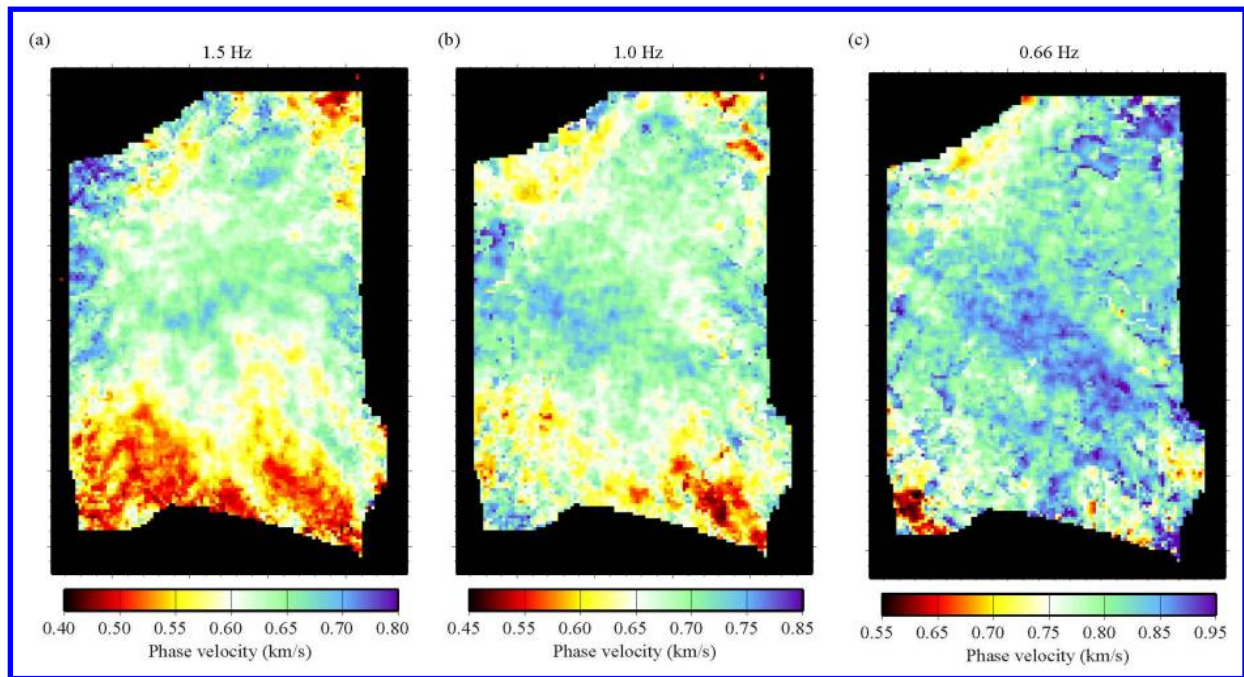
Figure 5. Rayleigh wave phase velocity maps at 1.5 Hz, 1.0 Hz, and 0.66 Hz.

For each virtual source, by calculating the spatial gradient of the phase travel time surface, Rayleigh wave phase velocity can be measured at each location based on eq. (2). The phase velocity measurements at each location based on different virtual sources are then averaged to suppress error in each individual measurement.

The resulting phase velocity maps for three frequencies are shown in Figure 5. The 1.5, 1.0, and 0.66 Hz Rayleigh wave phase velocity maps are particularly sensitive to shear velocity structures above 300-, 400-, and 600-meter depth respectively. The maps show a lot of detail, and matches well with the cross sections shown in Wright (1991). In the 1.5 Hz phase velocity map, clear slow anomaly is observed near the coast in the south which is likely corresponding to the loose sediments and potentially higher water saturation at the shallowest depth in this area. In the 0.66 Hz map, on the other hand, the most striking feature is the fast anomaly associate with the Newport-Inglewood Fault Zone (Figure 1). These 2D phase velocity maps at different frequency will be the foundation for future 3D inversion.

Conclusions

In this study, we demonstrate the potential of utilizing the cross-correlation of ambient noise to form a detailed shallow velocity function with a dense exploration array. Unlike the ambient noise tomography method applied on a much larger scale, we not only observe surface waves to a

higher frequency (0.2-10 Hz) range but also show clear evidence of body wave signals. While the body waves are relatively weak in each individual cross-correlation and stacking over different paths is required to enhance the signal, we are optimistic that the body wave signals will be further enhanced when we complete processing the full 6-months data.

The 2D Rayleigh wave phase velocity maps constrained based on travel time measurements and Eikonal tomography show correlation between observed velocity anomalies and known surface features such as the shallow slow anomaly associated with the southern coast and the fast anomaly associated with the Newport-Inglewood fault zone. The next step is to use the dispersion property of surface waves, to determine the velocity structure at different depths (Hermann, 1987). Inverting 3D velocity structure by involving both surface wave and body wave measurements will be the focus of future study.

Acknowledgements

EDITED REFERENCES
Note: This reference list is a copy-edited version of the reference list submitted by the author. Reference lists for the 2012
SEG Technical Program Expanded Abstracts have been copy edited so that references provided with the online metadata for
each paper will achieve a high degree of linking to cited sources that appear on the Web.

REFERENCES

Bensen, G. D., M. H. Ritzwoller, M. P. Barmin, A. L. Levshin, F. Lin, M. P. Moschetti, N. M. Shapiro, and Y. Yang, 2007, Processing seismic ambient noise data to obtain reliable broad-band surface wave dispersion measurements: Geophysical Journal International, **169**, 1239–1260, doi: 10.1111/j.1365-246X.2007.03374.x.

Draganov, D., X. Campman, and J. Thorbecke, 2006, Seismic interferometry: reconstructing the earth's reflection response: Geophysics, **71**, no. 4, S161–S170.

Draganov, D., X. Campman, J. Thorbecke, A. Verdel, and K. Wapenaar, 2009, Reflection images from ambient seismic noise: Geophysics, **74**, no. 5, A63–A67, doi: 10.1190/1.3193529.

Herrmann, R. B., 1987, Computer programs in seismology: St. Louis University.

Lin, F.-C., M. P. Moschetti, and M. H. Ritzwoller, 2008, Surface wave tomography of the western United States from ambient seismic noise: Rayleigh and Love wave phase velocity maps: Geophysical Journal International, **173**, 281–298, B12310, doi: 10.1111/j1365-246X.2008.03720.x.

Lin, F.-C., M. H. Ritzwoller, and R. Snieder, 2009, Eikonal tomography: Surface wave tomography by phase-front tracking across a regional broad-band seismic array: Geophysical Journal International, **177**, 1091–1110.

Lin, F.-C., M. H. Ritzwoller, J. Townend, S. Bannister, and M. K. Savage, 2007, Ambient noise Rayleigh wave tomography of New Zealand: Geophysical Journal International, **170**, 649–666, doi: 10.1111/j.1365-246X.2007.03414.x.

Lin, F.-C., M. H. Ritzwoller, Y. Yang, M. P. Moschetti, and M. J. Fouch, 2011, Complex and variable crustal and uppermost mantle seismic anisotropy in the western United States: Nature Geoscience, **4**, 55–61.

Lobkis, O. I., and R. L. Weaver, 2001, On the emergence of the Green's function in the correlations of a diffuse field: Journal of the Acoustical Society of America, **110**, 3011–3017.

Prieto, G. A., M. Denolle, J. F. Lawrence, and G. C. Beroza, 2011, On the amplitude information carried by ambient seismic field: Comptes Rendus Geoscience, **343**, 600–614.

Moschetti, M. P., M. H. Ritzwoller, and F.-C. Lin, 2010, Seismic evidence for widespread crustal deformation caused by extension in the western USA: Nature, **464**, 885–889.

Poli, P., H. A. Pedersen, M. Campillo, and the POLENET/LAPNET Working Group, 2012, Emergence of body waves from cross-correlation of short period seismic noise: Geophysical Journal International, **188**, 549–558, doi: 10.1111/j.1365-246X.2011.05271.x.

Ritzwoller, M. H., F.-C. Lin, and W. Shen, 2011, Ambient noise tomography with a large seismic array: Comptes Rendus Geoscience, **343**, 558–570, doi: 10.1016/j.crte.2011.03.007.

Ruigrok, E., X. Campman, and K. Wapenaar, 2011, Extraction of P-wave reflections from microseisms: Comptes Rendus Geoscience, **343**, 512–525, doi: 10.1016/j.crte.2011.02.006.

Sabra, K., P. Gersoft, P. Roux, and W. Kuperman, 2005, Extracting time-domain Green's function estimates from ambient seismic noise: Geophysical Research Letters, **32**, L03310, doi: 10.1029/2004GL021862.

Shapiro, N. M., M. Campillo, L. Stehly, and M. H. Ritzwoller, 2005, High resolution surface wave tomography from ambient seismic noise: Science, **307**, 1615–1618.

Smith, W. H. F., and P. Wessel, 1990, Gridding with continuous curvature splines in tension: Geophysics, **55**, 293–305.

Snieder, R., 2004, Extracting the Green's function from the correlation of coda waves: A derivation based on stationary phase: Physical Review E, **69**, 046610.

Stehly, L., M. Campillo, and N. Shapiro, 2006, A study of seismic noise from its long-range correlation properties: Journal of Geophysical Research, **111**, B10306, doi: 10.1029/2005JB004237.

Wright, T., 1991, Structural geology and tectonic evolution of the Los Angeles Basin, California, overview, *in* K. T. Biddle, ed., Active margin basins: AAPG Memoir 52, 35–134.

Zhan, Z., S. Ni, D. Helmberger, and R. Clayton, 2010, Retrieval of Moho-reflected shear wave arrivals from ambient seismic noise: Geophysical Journal International, **182**, 408–420, doi: 10.1111/j.1365-246X.2010.04625.x.